And., Intl.,J., Appl Sci., Eng., Tech, Vol 06, No 03, November 2026
e-ISSN: 2797-0442

Experimental Analysis of the Effect of Waste Heat Recovery on the Operational Performance of a Heat Pump Dryer

Solomzi Marco Ngalonkulu*, Amiyou Manaka
Department of Mechanical and Mechatronics Engineering, Tshwane University of Technology, South Africa

*Corresponding author, e-mail: ngalonkulus@tut.ac.za

Abstract—Air-source heat pump drying (ASHPD) systems are recognised for their energy efficiency, utilising ambient air as a low-grade energy source for moisture removal in agricultural products. However, climatic conditions significantly affect their thermodynamic performance, influencing both energy consumption and coefficient of performance (COP). This study experimentally evaluated an ASHPD system with waste-heat recovery across ambient temperatures ranging from 20 °C to −10 °C, under open, semi-closed, and fully closed air-loop configurations. Results indicate that waste-heat recovery increased evaporator temperatures by 1.5 °C in the semi-closed system and 9.4 °C in the fully closed system, leading to heating capacity improvements of 6.7% and 30.7%, respectively. Consequently, COP increased by 4.2% and 16.9%. However, high condenser pressure in the fully closed configuration restricted operation to ambient temperatures above 10 °C. As ambient temperature decreased, COP degradation was observed: 29.6% in the open system, 29.7% in the semi-closed system, and 19.9% in the fully closed system. These findings highlight the effectiveness of waste-heat recovery in improving ASHPD performance and mitigating efficiency losses under cold conditions, while emphasising the importance of selecting appropriate air-loop configurations based on climate.

Keywords: Heat pump drying, waste heat recovery, surrounding temperature, thermal performance, COP.

This article *is licensed under the CC–BY-SA license.*

1. Introduction

Drying processes are critical across various industries, notably in agriculture, food processing, and manufacturing, due to their significant impact on product quality and energy consumption. Traditional drying methods, often reliant on direct or indirect combustion of fossil fuels, entail substantial energy inefficiencies and environmental concerns [1]. Hence, the utilisation of alternative fuels and energy sources in drying processes is essential to promote sustainability and mitigate the environmental impact of fossil fuel combustion [2], [3]. Therefore, adopting energy-efficient drying technologies is crucial to reducing reliance on fossil fuels and advancing sustainable practices in drying applications [4]. In response, heat pump drying (HPD) systems have emerged as a promising alternative, offering improved energy efficiency and reduced environmental footprint [5], [6]. Among these, air-source heat pump drying systems have attracted attention for their potential to harness surrounding air as a heat source, thereby reducing operational costs and environmental impact [7], [8], [9].

Nevertheless, the performance of ASHPD systems is heavily influenced by surrounding temperatures, directly affecting their efficiency and all operating parameters [10], [11], [12]. According to Sezen [13], the performance of ASHPD systems is closely related to the refrigerant's evaporation and condensation temperatures, as these temperatures are directly influenced by the inlet air temperatures entering the evaporator and condenser, which are equipped with fan-assisted finned-tube heat exchangers. As such, a study by Ngalonkulu and Huan [14] on the open-loop ASHPD system reported a significant drop in thermal performance as surrounding temperatures decreased. Additionally, the

Received: May 25, 2026, Revised: July 2, 2026, Accepted: October 9, 2026
https://doi.org/10.25077/aijaset.v6i3.353

literature shows that the thermal performance of an ASHP system with a finned-tube heat exchanger can be significantly enhanced by raising the surrounding temperature, thereby improving the inlet air temperature to the evaporator. Since ambient temperature, airflow velocity, and frost formation critically influence HPD efficiency, COP, and drying rates, designs such as solar-assisted augmentation and waste-heat integration can mitigate the effects of environmental variability. Although the influence of surrounding temperature on heat pump dryer performance has been recognised, limited attention has been given to investigating system designs that dynamically adapt to varying environmental conditions.

Lamidi, Jiang, Pathare, Wang and Roskilly [15] suggest that enhancing the efficiency of a HPD system can be accomplished through methods such as insulation, heat recovery, recirculation, and adjusting the system's operating parameters. Therefore, optimising HPD systems by considering waste heat recovery and temperature differentials can lead to improved drying performance, energy efficiency, and overall system effectiveness [16], [17]. Huang, Zheng, Baleynaud and Lü [18] analysed the feasibility of waste heat recovery technologies such as heat pumps, heat exchangers, and heat storage systems for capturing low-temperature waste heat and implementing simple heat recovery systems and utilising the recovered energy to preheat fresh inlet air, which has been shown by Ghasemkhani, Keyhani, Aghbashlo, Rafiee and Mujumdar [19] to improve the exergetic performance of air dryers. Moreover, the incorporation of a waste heat recovery system featuring temperature-differential control and recirculation strategies reduces specific energy consumption and improves exergy efficiency [10], [20]. Furthermore, Table 1 provides a summary of various heat pump drying systems with waste heat recovery techniques.

Table 1. Summary of performance of some heat pump drying systems with waste heat recovery

Author	Application	Waste heat recovery approach	Operating temperature	Notable findings
Haibo and Kun [21]	Agricultural produce (General)	Waste heat recovery heat exchanger integrated into the heat pump drying system.	-5 to 25 °C	Ambient conditions strongly influence HPD performance. Waste heat recovery increased with Relative Humidity. Also the ambient meteorological variation substantially alters heat recovery, power use, COP, and SMER
Fu, Shi, Yuan, Zhang and Sun [22]	Paddy drying	Sensible heat from moist air by pre-heating the cold-dry air exiting the evaporator with the warm-moist air from the drying chamber.	25 °C	Adding heat recovery to the closed-cycle heat pump drying system improved SMER. An increase in condensing temperature reduces COP and SMER.
Naemsai, Jareanjit and Thongkaew [23]	Chilli pepper	Enclosed evaporation and condensation chambers of the HPD.	Not specified	The heat recovery system significantly improved the drying efficiency, coefficient of performance (COP), and specific energy consumption (SEC) compared to the SAHPD without heat recovery.
Wang, Li, Qiu, Yu, Luo, Li and Ma [24]	Mango drying	The exhaust moist air from the drying cabinet was blown through the heat exchanger, then passed through the evaporator of the heat pump, and subsequently discharged.	20 °C	improved COP and reduced power consumption compared to a standalone heat pump drying system

Despite the potential benefits of employing heat pump systems for drying, the existing literature highlights numerous system configurations and control strategies but emphasises that design and operational parameters are typically tuned case-by-case rather than optimised systematically, particularly with respect to specific ambient conditions [25], [26], [27]. Hence, there remains a gap in understanding the optimal configurations and operational parameters that maximise the efficiency of ASHPD systems at specific environmental conditions. Hence, this study aims to experimentally evaluate the influence of heat recovery on the thermal performance of an air-source heat pump drying system. By investigating open, semi-closed, and closed configurations, this research seeks to provide comprehensive insights into the impact of waste-heat recovery on evaporator temperatures, heating capacity, and overall COP. The findings from this study underscore the critical role of waste heat recovery in mitigating COP degradation in cold conditions and emphasise the need for tailored air-loop configurations to optimise HPD system performance under varying weather conditions.

2. Method

2.1 Heat pump dryer system

The ASHPD system test rig, equipped with air-to-air crossflow heat exchangers, was designed to operate in three configurations: open, semi-closed, and fully closed, as shown in Figure 1(b). The system consisted of a compressor, condenser, thermal expansion valve (TEV), and evaporator. The heating and cooling capacities of the condenser and evaporator were 3.2 kW and 2.4 kW, respectively. The test rig utilised a 0.5 kW semi-hermetic compressor with a maximum static pressure limit of 20.5 bar. An externally equalised thermal expansion valve with a Ø1.51mm orifice insert was used for refrigerant expansion, and R134a was the refrigerant employed in the system. These air ducts, with a 205 x 250 mm cross-sectional area, were constructed from 1.2 mm-thick galvanised metal sheets and connected the heat exchangers to the drying chamber, which measured 900 mm x 500 mm x 650 mm and featured a hinged lid for easy loading and unloading. The entire system was insulated with a 20 mm-thick layer of polyurethane foam to reduce heat loss.

In the fully open configuration, flaps A, B, C, and D are open, while air dampers (parts 5 and 10) are closed. In this setup, fresh air on the high-temperature side of the HPD is drawn into the system at point A by the condenser fan. The condenser heats the air before passing it into the drying chamber. The hot air from the drying chamber is then released into the surrounding environment at point B. On the evaporator side, fresh air from the surrounding environment is drawn into the system at point C, passes through the evaporator as a heat source for the HPD system, and is discharged back into the surrounding environment at point D.

In the semi-closed configuration (Figure 1a), air flaps B and C are closed, and the air damper (part 5) is open while damper 10 remains closed. Just like in the open configuration, fresh air on the high-temperature side of the HPD is drawn into the system at point A by the condenser fan. The condenser heats the air before passing it into the drying chamber. The hot air from the drying chamber is then directed to the evaporator for heat recovery, and the cooler air from the evaporator is discharged to the surrounding environment at point D.

In the fully closed configuration, the HPD system recirculates the air through the evaporator, condenser, and drying chamber. The heated air from the condenser is directed into the drying chamber, facilitating moisture absorption from the material being dried. The humid air is then directed to the evaporator, where heat is harvested to elevate the evaporator temperature. After cooling in the evaporator, the air is reheated by the condenser to increase its capacity to hold more water vapour at the set drying temperature before being returned to the drying chamber, and the cycle repeats continuously.

To achieve synchronised speeds and maintain uniform air velocities throughout the heat exchangers in all configurations, the condenser and evaporator fans were connected in parallel to a single Danfoss VLT2800 variable-speed drive. This setup ensured coordination between the two heat exchanger fans, particularly in the semi-closed and fully closed HPD system configurations, promoting optimal performance and efficiency across different operating modes.

Various parameters of the HPD system, including temperature, pressure, refrigerant mass flow rate, and power consumption, were systematically measured and recorded at multiple locations within the system using the CompactDAQ data acquisition system (Figure 1a).

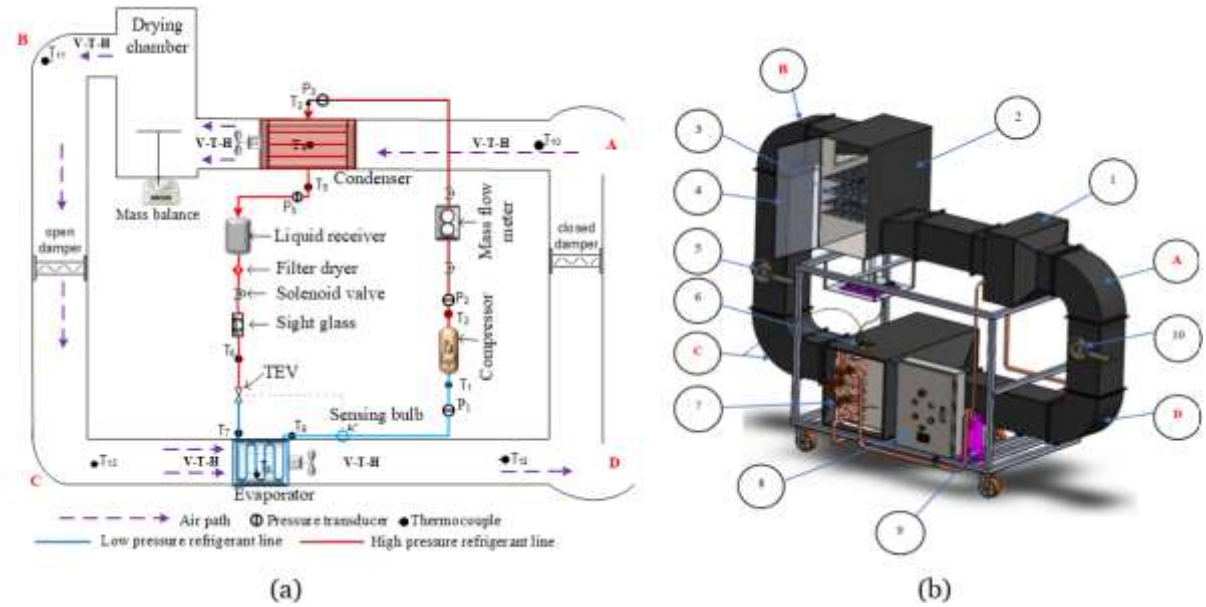


Figure 1. Schematic of the HPD in closed configuration. Air flaps (A, B, C, D), condenser (1), drying chamber (2), drying trays (3), dryer lid (4), air damper (5), data acquisition system (6), evaporator (7), control panel (8), liquid receiver (9), air damper (10)

2.2 Measurement instruments

This study utilised 4 pressure transducers, 15 T-type thermocouples, and 5 hot-wire air velocity/temperature sensors. The sensors were positioned within the test rig to precisely measure the system's parameters, including refrigerant temperatures and pressures on both the low and high-pressure sides, ambient air temperature, air temperature and velocity across the evaporator and condenser, as well as air temperature at the suction and discharge of the HPD system, in accordance with ASHRAE standards.

A Coriolis mass flow meter was strategically placed downstream of the compressor to ensure precise measurement of the refrigerant mass flow rate, thereby guaranteeing that only gaseous refrigerant was included in the measurements. The Coriolis mass flow meter functioned effectively over a range of fluid temperatures from -50 °C to 150 °C, ambient temperatures from -20 °C to 70 °C, and a maximum pressure of 25 MPa. The measurement capacity ranged from 0 to 100 kg/h, with the manufacturer's claimed accuracy of ±0.2% at full scale and repeatability of ±0.1%.

Type-T thermocouples, capable of measuring temperatures from -65 °C to 130 °C with an accuracy of ±1 °C, were used to measure temperatures at different locations within the HPD system. Pressure measurements on both the low- and high-pressure sides of the HPD system were conducted utilising WIKA pressure transducers, which possess a relative uncertainty of 0.1% at full scale. The

sensors generate a current output signal ranging from 4 to 20 mA. This signal is then processed by the CompactDAQ data acquisition system and sent to a computer operating LabVIEW (2019) through a USB connection.

2.3 Experimentation

Initially, temperature and pressure measurements were recorded and analysed to confirm the accuracy and proper functioning of the measuring instruments before each experiment. The environmental chamber was subsequently configured to operate under specific surrounding conditions to be investigated, which were 20 °C, 10 °C, 0 °C, and -10 °C and allowed to stabilise. Once stable conditions were achieved, the HPD system was operated for approximately 2 hours to adapt to the environment. Then, data were collected at 30-minute intervals over the 120-minute period following stabilisation, using a cross-sectional sampling method from the continuously recorded data. The average values of the primary recorded data, including temperature and pressure, were used to derive secondary data, particularly refrigerant properties such as enthalpies and densities.

2.4 Analysis of data

The heat pump performance metrics were obtained and computed using the Engineering Equation Solver (EES) software, V10.836-3D (2020). To determine the heating capacity of the HPD system, the enthalpy difference across the condenser was multiplied by the refrigerant mass flow rate, as specified in Equation (1). This method was used to determine the heat generated by the system, accounting for the enthalpy change across the condenser and the refrigerant mass flow rate.

$$\dot{Q}_{cond} = \dot{m}_{ref}(h_2 - h_4) \tag{1}$$

where h_2 is the specific enthalpy of the refrigerant at the condenser inlet (kJ/kg), h_4 is the specific enthalpy of the refrigerant at the condenser exit (kJ/kg), and $\dot{m}_{ref}$ is the refrigerant mass flow rate (kg/s).

The overall coefficient of performance is given by the heating capacity to the total power consumed by the system, encompassing the power usage of the evaporator and condenser fans along with the compressor, as outlined in Equation (2).

$$COP_{HPD} = \frac{\dot{Q}_{cond}}{(P_{comp} + P_{fan,cond} + P_{fan,evap})} \tag{2}$$

where P_{fan} is the power consumption by the evaporator and condenser fans.

2.5 Experimental uncertainties

An uncertainty analysis is necessary to demonstrate the repeatability and precision of the experimental data [19]. Experimental errors and uncertainties in research can arise from various factors, including instrument selection conditions, calibration procedures, environmental influences, reading and recording methods, and test planning strategies [28], [29]. The uncertainties of the results in this study were calculated using the Root-Sum-Squared (RSS) method shown in Equation (3), developed by Holman [30].

$$U = \left[\left(\frac{\partial F}{\partial z_1}u_1\right)^2 + \left(\frac{\partial F}{\partial z_2}u_2\right)^2 + \ldots + \left(\frac{\partial F}{\partial z_n}u_n\right)^2\right]^{1/2} \tag{3}$$

3. Results and Discussion

3.1 Effect of waste heat recovery on the evaporator temperature

The influence of waste heat recovery from the drying chamber on the evaporator temperature at surrounding temperatures of -10 °C, 0 °C, 10 °C, and 20 °C is depicted in Figure 2. Notably, due to increased heat input from the ambient environment, the evaporator temperature increased continuously as the ambient temperature rose across all three HPD configurations. Moreover, as ambient temperatures increased, the difference between the open and semi-closed evaporator temperatures increased from 0.2 °C to 3.5 °C due to the higher heat input from the surrounding environment. Subsequently, the recovery of waste heat through semi-closed HPD configurations had a smaller effect on increasing evaporator temperatures, especially at surrounding temperatures of 0 °C and below, with an average increase of 1.5 °C compared to an open-loop configuration. However, the fully closed HPD configuration has resulted in a 9.0 °C increase in the evaporator temperatures. In all three configurations, the evaporator temperature steadily increased as ambient temperatures increased, and the heat recovery from the drying chamber resulted in a noticeable increase in evaporator temperatures. The waste heat recovered from the drying chamber is transferred to the evaporator, enabling heat absorption from both the low-temperature ambient air and the relatively warmer exhaust air stream. This increases the heat flux into the evaporator, raising both the refrigerant enthalpy gain and the evaporating temperature, thereby increasing the evaporator load. For instance, at a surrounding temperature of 20 °C, the open configuration reached a peak of 7.3 °C, while the semi-closed configuration reached a peak of 10.8 °C. In the fully closed configuration, the evaporator temperature reached 8.5 °C at an ambient temperature of 10 °C. These findings correspond with a recent prediction model for a DX-SAHP, which found that evaporation temperature increases by about 0.58 °C for every 1°C increase in ambient temperature [31].

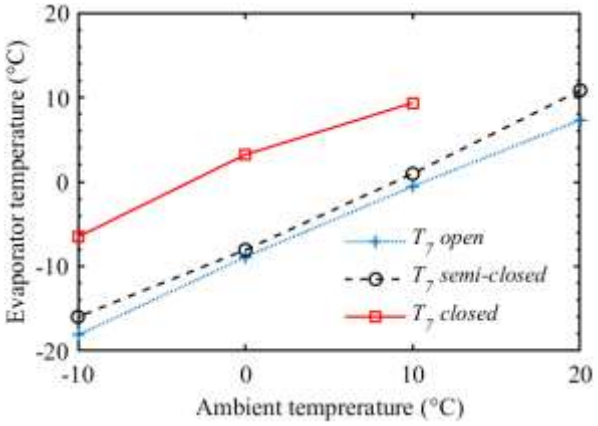


Figure 2. Effect of heat recovery on evaporator temperature

3.2 Effect of waste heat recovery on the suction temperature and pressure

The effect of waste-heat recovery from the drying chamber through the semi-closed and fully closed configurations on the suction temperature is illustrated in Figure 3a. By harnessing waste heat from the drying chamber in the fully closed setup, a 239.4% increase in suction temperature was observed, rising from 5.5 °C to 18.8 °C compared to the open-loop configuration. The results also showed a 92.2% increase in suction temperature in the closed-loop configuration compared to the semi-closed setup at a surrounding temperature of 10 °C. Similarly, the semi-closed HPD configuration demonstrated a notable increase in suction temperature. At a surrounding temperature of 20 °C, the HPD

configuration reached a peak suction temperature of 19.8 °C, a 52.4% increase compared to the open-loop configuration. The suction temperatures increased as the surrounding temperatures rose.

The variation in compressor suction pressure with waste heat recovery across different ambient temperatures is shown in Figure 3b. Due to rising ambient temperatures, which increase thermal input to the evaporator and heat recovery from the drying chamber, higher evaporator temperatures lead to higher compressor suction temperatures and pressures. As a result, the suction pressure increased substantially in both the semi-closed and fully closed configurations compared to the open configuration. Particularly, the suction pressure increased by 8.3% in the semi-closed configuration and by 38.3% in the fully closed configuration compared to the open configuration. Notably, the evaporator's recovery of waste heat significantly improved the compressor's suction conditions, especially in the closed-loop configuration. However, higher suction conditions can lead to higher operating temperatures and shorten the compressor's service life.

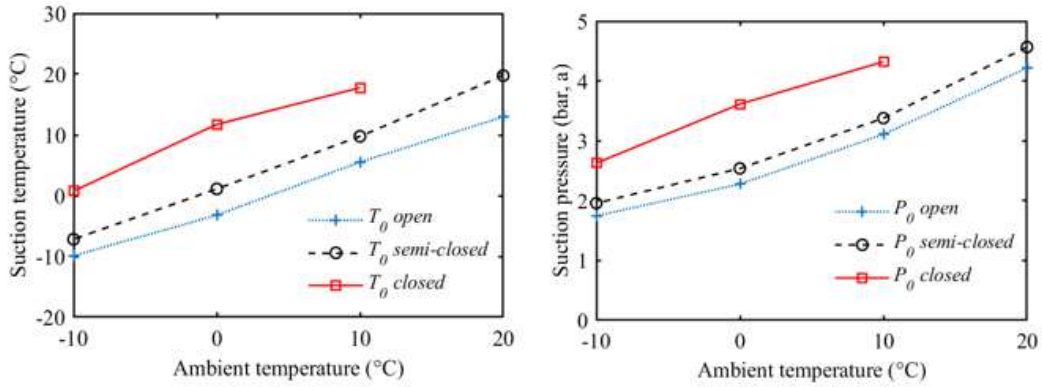


Figure 3. Variation of suction temperatures (a), and pressures (b) with surrounding temperature

Figure 4a and 4b illustrate the changes in discharge temperature and pressure as waste heat was recovered from the drying chamber. Notably, at 10 °C, the semi-closed configuration showed a modest 2.3% increase in discharge temperature compared to the open-loop system. In contrast, the fully closed configuration displayed higher discharge temperatures of 89.8 °C, exceeding those of the semi-closed and open configurations by 13.9% and 16.6%, respectively. Likewise, discharge pressures increased with higher surrounding temperatures and heat recovery, due to the reduced temperature difference between the HPD system and the surrounding environment. The semi-closed configuration recorded a 6.4% increase, while the fully closed configuration attained a 38.3% increase over the open-loop configuration. The reduced temperature difference between the condenser unit and the surrounding temperatures lowered the heat rejection from the condenser, resulting in higher discharge pressures, especially in the fully closed configuration.

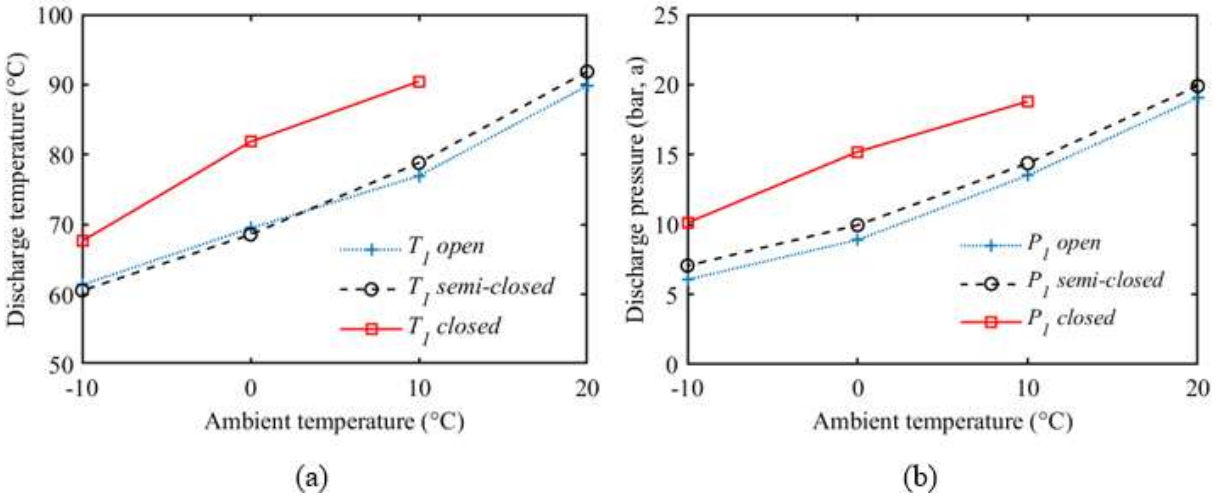


Figure 4. Variation in discharge temperature (a) and pressure (b) with surrounding temperature

3.3 Effect of waste heat recovery on the compression ratio and volumetric efficiency of the compressor

Although the suction and discharge pressures increased with increased surrounding temperatures owing to the high thermal energy associated with the heat recovered by the evaporator, and were higher in the fully closed and semi-closed configurations than in the open-loop configuration, the compression ratio moderately increased with surrounding temperature for all configurations, as depicted in Figure 5a. Surprisingly, at a surrounding temperature of 10 °C, the open-loop configuration achieved the highest compression ratio of 4.4, while the semi-closed and fully closed configurations reached a compression ratio of 4.3. The reduced compression ratio in the semi-closed and fully closed configurations was due to a higher rate of increase in suction pressure than in discharge pressure. The increasing compression ratio with surrounding temperatures negatively affected the volumetric efficiency of the compressor for all three HPD configurations examined. Similarly, due to higher discharge pressures in the fully closed and semi-closed configurations, their volumetric efficiencies were lower, as shown in Figure 5b.

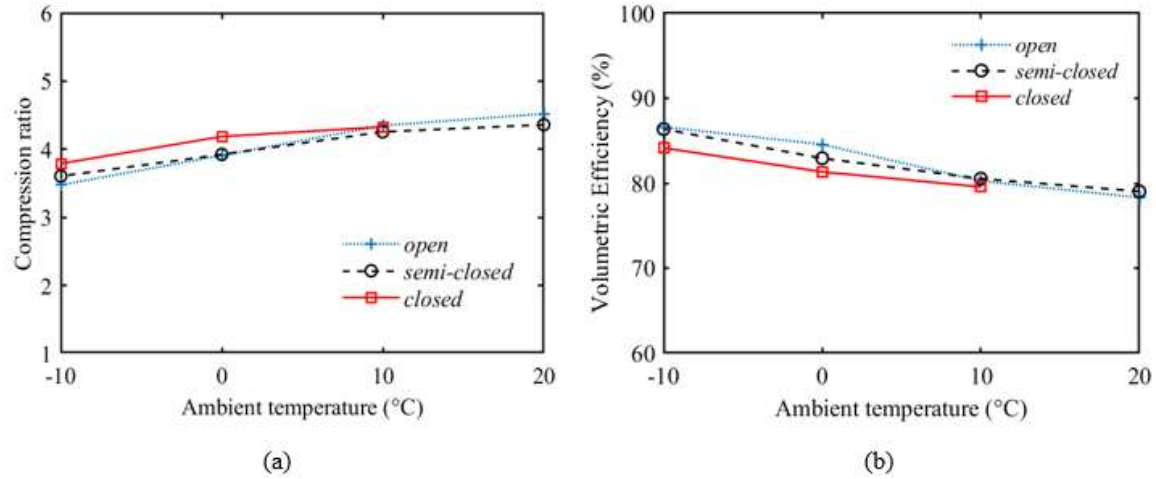


Figure 5. Effect of surrounding temperature on compression ratio (a) and volumetric efficiency (b)

3.4 Variation of compression work and power input with surrounding temperatures

Figure 6 compares the compression work of the open, semi-closed, and fully closed configurations at varied surrounding temperatures. The compression work increased with higher surrounding temperatures in all three configurations examined, due to higher refrigerant density. Moreover, the compression work was higher with the fully closed configuration, reaching a maximum of 0.78 kJ/s at

a surrounding temperature of 10 °C, while the semi-closed and open configurations recorded maximum values of 0.85 kJ/s and 0.81 kJ/s at a surrounding temperature of 20 °C, respectively. Due to the higher refrigerant mass flow rates observed with the closed and semi-closed configurations, the compression work to push through the higher refrigerant quantity was higher. Subsequently, the compressor's power input increased with increasing compression work, as shown in Figure 7.

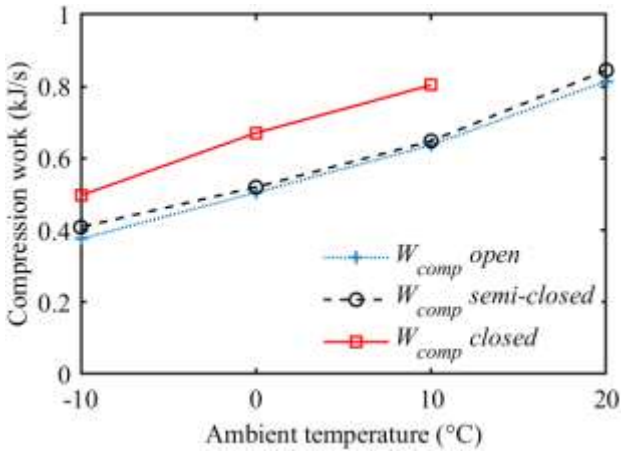


Figure 6. Comparison of the effect of the surrounding temperature on the compression work

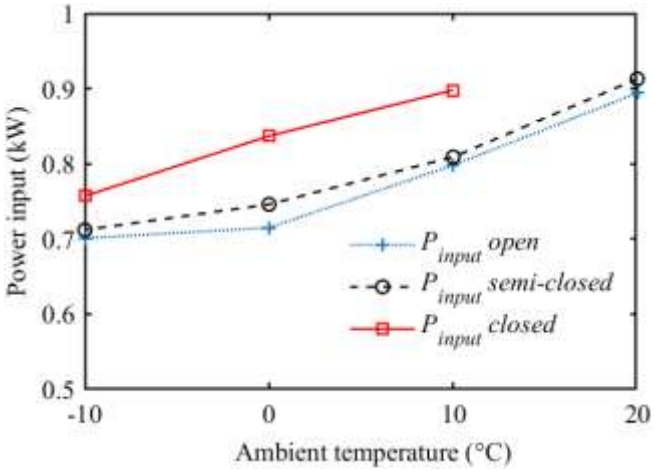


Figure 7. Comparison of the influence of the surrounding temperature on the power input

3.5 Comparison of heating capacity and overall COP at varied surrounding temperatures

As illustrated in Figure 8, the heating capacity increased with increased surrounding temperature. Effectively recovering waste heat from the drying chamber in the fully closed configuration resulted in a 24.7% improvement in heating capacity compared to the open-loop configuration. In contrast, the heating capacity in the semi-closed configuration increased by 11.6% compared to the open configuration. Since the overall COP is the ratio of heating capacity to the total power consumed by the HPD system. The heating capacity increased with ambient temperature, and in the fully closed and semi-closed configurations, it increased at a greater rate than the corresponding compressor power, resulting in a significantly improved COP, as depicted in Figure 9. Similar results were reported by Naemsai, Jareanjit and Thongkaew [23]. Also, it is worth noting that the open-loop configuration exhibited the lowest overall COP, reaching 3.24 at 20 °C and 3.18 at 10 °C. On the other hand, the semi-closed configuration exhibited the second-highest COP values, achieving 3.65 at 20 °C and 3.32 at 10 °C, while the fully closed configuration achieved the highest COP of 3.73 at 10 °C. The findings of this study indicate that heat recovery from the drying chamber by the evaporator enhanced the overall COP by 9% and 17.2% in the semi-closed and fully closed configurations, respectively.

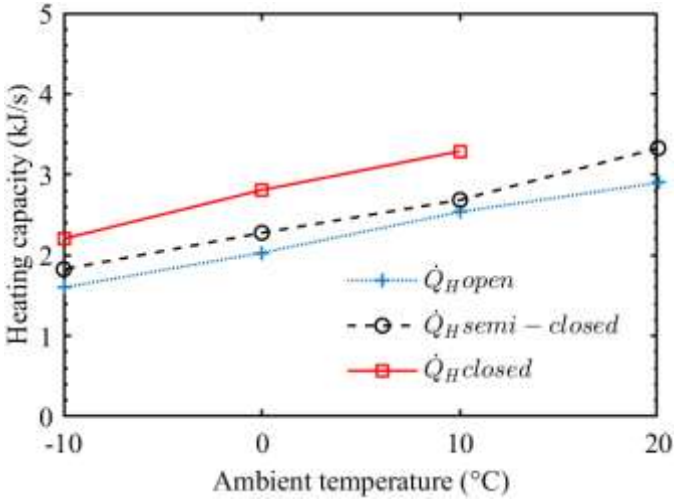


Figure 8. Comparison of the effect of the surrounding temperature on the heating

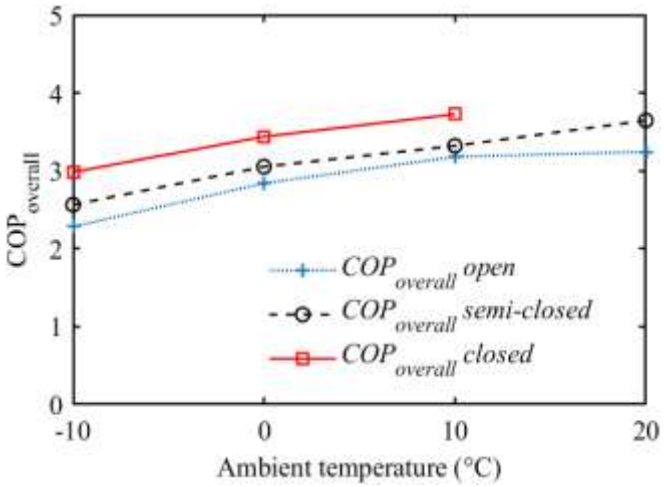


Figure 9. Comparison of the effect of the surrounding temperature on the overall COP

3.6 Comparison of drying temperature at varied surrounding temperatures

Figure 10 shows the effect of ambient temperature on the drying temperature for open, semi-closed, and fully closed HPD system configurations. Due to the lower condenser temperatures, the drying temperatures in the open-loop setup were the lowest, peaking at 42.3 °C at an ambient temperature of 20 °C, while the semi-closed configuration reached a maximum of 46.1 °C at the same surrounding temperature. A 10 °C drop in the surrounding temperature, from 20 °C to 10 °C, resulted in a 33.7% reduction in drying temperatures for both the semi-closed and open-loop configurations. The drying temperature dropped by 15.6 °C in the semi-closed setup, going from 46.1 °C to 30.5 °C.

Nevertheless, at 10 °C, the fully closed configuration achieved a maximum drying temperature of 40.3 °C, which was 32.1% and 43.4% higher than in the semi-closed and open-loop configurations, respectively. A further decrease in surrounding temperature from 10 °C to 0 °C detrimentally affected the drying temperatures of the semi-closed and open-loop configurations, resulting in a combined average decrease of 50.5%. Remarkably, the drying temperature of the fully closed configuration decreased by only 24.1% from 39.8 °C to 30.2 °C over the same temperature range, making it the appropriate configuration for low ambient temperatures.

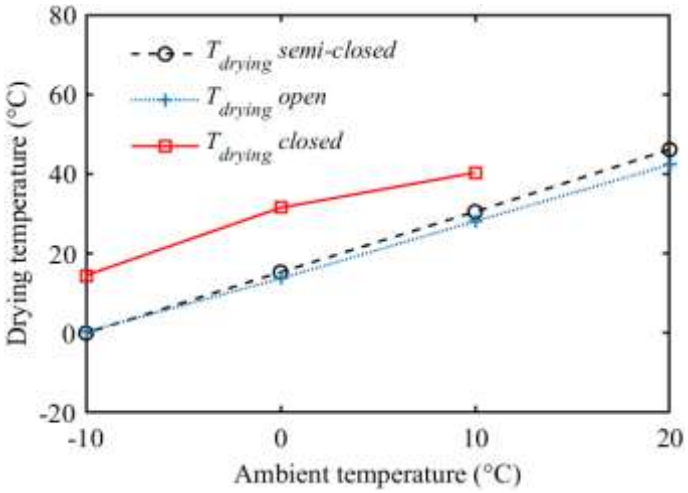


Figure 10. Comparison of the impact of the surrounding temperature on the drying temperatures

4. Conclusion

The findings of this study suggests that ambient temperature is a critical factor influencing the thermal performance of the heat pump drying system. Higher ambient temperatures resulted in increased compressor discharge temperatures, mainly due to reduced heat rejection in the condenser. Overall, the open-loop and semi-closed configurations achieved their best performance at 20 °C, whereas the closed configuration was limited to 10 °C because of the higher operating conditions associated with this mode. A reduction in ambient temperature led to a decline in drying air temperature across all configurations. The decrease was particularly evident in the semi-closed and open-loop arrangements, where drying air temperatures dropped by 42 °C and 46.1 °C, respectively, as ambient temperature decreased from 20 °C to -10 °C. In the closed configuration, the drying air temperature decreased by 26.1 °C from a maximum of 39.8 °C as the surrounding temperature dropped from 10 °C to -10 °C.

Although the integration of waste heat recovery through the semi-closed configuration produced a marginal improvement in the overall coefficient of performance, its effect on drying temperature improvement under adverse ambient conditions was limited. The results therefore indicate that the semi-closed configuration is most beneficial for energy-saving applications at ambient temperatures of 20 °C and above. Conversely, the fully closed configuration is better suited to lower surrounding temperatures, as its higher operating conditions enable more stable performance under colder operating environments. These findings highlight the importance of selecting the appropriate heat pump dryer configuration according to the prevailing ambient conditions and the required thermal performance of the drying process.

Acknowledgment

This work was supported in part by the National Research Foundation (NRF) of South Africa under Grant Ref Numbers: BAAP2204254744.

References

[1] F. Perera, “Pollution from fossil-fuel combustion is the leading environmental threat to global pediatric health and equity: Solutions exist,” *International journal of environmental research and public health*, vol. 15, no. 1, pp. 16, 2018.

[2] D. Archer, M. Eby, V. Brovkin, A. Ridgwell, L. Cao, U. Mikolajewicz, K. Caldeira, K. Matsumoto, G. Munhoven, and A. Montenegro, “Atmospheric lifetime of fossil fuel carbon dioxide,” *Annual review of earth and planetary sciences*, vol. 37, no. 1, pp. 117–134, 2009.

[3] Á. Calín-Sánchez, L. Lipan, M. Cano-Lamadrid, A. Kharaghani, K. Masztalerz, Á. A. Carbonell-Barrachina, and A. Figiel, "Comparison of Traditional and Novel Drying Techniques and Its Effect on Quality of Fruits, Vegetables and Aromatic Herbs," *Foods,* vol. 9, no. 9, pp. 1261, 2020.
[4] K. A. Metwally, A. A. T. Oraiath, I. Elzein, T. M. El-Messery, C. Nyambe, M. M. Mahmoud, M. A. Abdeen, A. A. Telba, U. Khaled, and A. Beroual, "The Mathematical Modeling, Diffusivity, Energy, and Enviro-Economic Analysis (MD3E) of an Automatic Solar Dryer for Drying Date Fruits," *Sustainability,* vol. 16, no. 8, pp. 3506, 2024.
[5] M. Reppich, Z. Jegla, J. Grondinger, Y. O. Azouma, and V. Turek, "Mathematical modeling of drying processes of selected fruits and vegetables," *Chemie Ingenieur Technik,* vol. 93, no. 10, pp. 1581–1589, 2021.
[6] X. Zhang, and K. Caldeira, "Time scales and ratios of climate forcing due to thermal versus carbon dioxide emissions from fossil fuels," *Geophysical Research Letters,* vol. 42, no. 11, pp. 4548–4555, 2015.
[7] K. Yousaf, K. Chen, and M. A. Khan, "An Introduction of Biomimetic System and Heat Pump Technology in Food Drying Industry," 2021.
[8] C. M. Mârza, R.-P. Moldovan, G. Corsiuc, and G. Chisăliță, "Improving the Energy Performance of a Household Using Solar Energy: A Case Study," *Energies,* vol. 16, no. 18, pp. 6423, 2023.
[9] B. Wei, Y. Wang, Z. Liu, and B. Liu, "Optimization Study on a Solar-assisted Air Source Heat Pump System With Energy Storage Based on the Economics Method," *International Journal of Energy Research,* vol. 44, no. 3, pp. 2023–2036, 2019.
[10] Z. Sun, J. Chen, T. Dai, Y. Wang, R. Liang, W. Liu, C. Liu, and L. Deng, "Recent Advances in Heat Pump Drying System for the Food Industry: Structure, System Optimization, Applications, and Prospects," *Comprehensive Reviews in Food Science and Food Safety,* vol. 24, no. 4, 2025.
[11] M. J. Huang, and N. Hewitt, "The Experimental Analysis of the Effect of Ambient Factors on the Defrosting of Economised Vapour Injection Compressor Air Source Heat Pump in Marine Climates," *International Journal of Refrigeration,* vol. 36, no. 3, pp. 820–827, 2013.
[12] T. Kropas, G. Streckienė, and J. Bielskus, "Experimental Investigation of Frost Formation Influence on an Air Source Heat Pump Evaporator," *Energies,* vol. 14, no. 18, pp. 5737, 2021.
[13] K. Sezen, "Operation Parameters Variation of Air Source Heat Pump According to the Outdoor Temperature," *Politeknik Dergisi,* vol. 26, no. 3, pp. 1179–1184, October, 2023.
[14] S. M. Ngalonkulu, and Z. Huan, "Viability of an Open-Loop Heat Pump Drying System in South African Climatic Conditions," *Energies,* vol. 17, no. 10, pp. 2432, 2024.
[15] R. O. Lamidi, L. Jiang, P. B. Pathare, Y. D. Wang, and A. P. Roskilly, "Recent advances in sustainable drying of agricultural produce: A review," *Applied Energy,* vol. 233-234, pp. 367–385, 2019/01/01/, 2019.
[16] H. Xu, "Performance Optimization Analysis of an Air-Source Heat Pump With Multi-Stage Waste Heat Recovery," *E3s Web of Conferences,* vol. 520, pp. 04009, 2024.
[17] M. A. R. Kavindi, K. S. P. Amaratunga, E. M. C. Ekanayake, A. J. Fernando, and A. M. S. K. Abesinghe, "CFD Simulation of Airflow Distribution in a Heat Pump-Assisted Deep-Bed Paddy Dryer," *Applied Engineering in Agriculture,* vol. 38, no. 1, pp. 1–8, 2022.
[18] F. Huang, J. Zheng, J. M. Baleynaud, and J. Lü, "Heat Recovery Potentials and Technologies in Industrial Zones," *Journal of the Energy Institute,* vol. 90, no. 6, pp. 951–961, 2017.
[19] H. Ghasemkhani, A. Keyhani, M. Aghbashlo, S. Rafiee, and A. S. Mujumdar, "Improving exergetic performance parameters of a rotating-tray air dryer via a simple heat exchanger," *Applied Thermal Engineering,* vol. 94, pp. 13–23, 2016/02/05/, 2016.
[20] A. Singh, J. Sarkar, and R. R. Sahoo, "Experiment on Waste Heat Recovery-assisted Heat Pump Drying of Food Chips: Performance, Economic, and Exergoeconomic Analyses," *Journal of Food Processing and Preservation,* vol. 44, no. 9, 2020.
[21] Z. Haibo, and W. Kun, "Annual performance analysis of heat pump drying system with waste heat recovery," *Sustainable Energy Technologies and Assessments,* vol. 53, pp. 102625, 2022/10/01/, 2022.
[22] H. Fu, J. Shi, J. Yuan, X. Zhang, and L. Sun, "Heat recovery scheme design and thermodynamic analysis of closed-cycle heat pump drying system," *Energy Conversion and Management,* vol. 286, pp. 117034, 2023/06/15/, 2023.

[23] T. Naemsai, J. Jareanjit, and K. Thongkaew, "Experimental investigation of solar-assisted heat pump dryer with heat recovery for the drying of chili peppers," *Journal of Food Process Engineering,* vol. 42, no. 6, pp. e13193, 2019/10/01, 2019.
[24] Y. Wang, M. Li, Y. Qiu, Q. Yu, X. Luo, G. Li, and X. Ma, "Performance analysis of a secondary heat recovery solar-assisted heat pump drying system for mango," *Energy Exploration & Exploitation,* vol. 37, no. 4, pp. 1377–1387, 2019/07/01, 2019.
[25] T. N. Roman, "Energy study of a heat pump used for air heating and dehumidification," *Engenharia Térmica (Thermal Engineering),* vol. 14, no. 2, pp. 12–17, 2015.
[26] S.M. Ngalonkulu, and Z. Huan, "The Thermal Analysis of a Semi-Open Heat Pump Drying System: An Experimental Investigation," in AIUE Proceedings of the 17th Industrial and Commercial Use of Energy Conference, The Riverclub, Cape Town, 2019.
[27] A. Graban, E. Groll, J. Braun, and D. Ziviani, "Review of heat pump tumble clothes dryer energy efficiency and related technologies," 2021.
[28] F. Zhu, H. Zhang, L. Huang, X. Li, and P. Feng, "Research on Absolute Calibration of GNSS Receiver Delay Through Clock-Steering Characterization," *Sensors,* vol. 20, no. 21, pp. 6063, 2020.
[29] D. Michalski, K. Strąk, and M. Piasecka, "Estimating Uncertainty of Temperature Measurements for Studies of Flow Boiling Heat Transfer in Minichannels," *Epj Web of Conferences,* vol. 213, pp. 02059, 2019.
[30] J. P. Holman, "Analysis of experimental data," *Experimental methods for engineers,* pp. 48–143, 2001.
[31] P. Yin, X. Kong, Z. Yue, H. Yu, Y. Li, and J. Li, "Evaporation temperature prediction of a direct-expansion solar-assisted heat pump," *Solar Energy,* vol. 256, pp. 215–224, 2023/05/15/, 2023.